N6-methyladenosine modification governs liver glycogenesis by stabilizing the glycogen synthase 2 mRNA

Xiang Zhang
the Fourth Military Medical University
Huilong Yin
Xinxiang Medical University https://orcid.org/0000-0002-1046-4787
Xiaofang Zhang
Fourth Military Medical University
Xunliang Jiang
the Fourth Military Medical University
Yongkang Liu
the Fourth Military Medical University
Yingran Peng
Fourth Military Medical University
Da Li
Fourth Military Medical University
Yanping Yu
Shaanxi Provincial Tumor Hospital
Jinbao Zhang
Fourth Military Medical University
Shuli Cheng
the Fourth Military Medical University
Angang Yang
State Key Laboratory of Cancer Biology, Department of Immunology, Fourth Military Medical University
https://orcid.org/0000-0002-8854-4672
Rui Zhang (ruizhang@fmmu.edu.cn)
Fourth Military Medical University https://orcid.org/0000-0002-6147-1573

Article

Keywords: N6-methyladenosine, Liver glycogen, Glycogenesis, Epigenetics, Glycogen synthase 2

Posted Date: December 13th, 2021

DOI: https://doi.org/10.21203/rs.3.rs-1117441/v1

Version of Record: A version of this preprint was published at Nature Communications on November 17th, 2022. See the published version at https://doi.org/10.1038/s41467-022-34808-2.

Abstract

Hepatic glycogen is the main source of blood glucose and controls the intervals between meals in mammals. Hepatic glycogen storage in mammalian pups is insufficient compared to their adult counterparts; however, the detailed molecular mechanism is poorly understood. Here, we showed that, similar to glycogen storage pattern, N6-methyladenosine (m6A) modification in mRNAs gradually increases during the growth of mice in liver. Strikingly, in the liver-specific Mettl3 knockout mice, loss of m6A modification disrupts liver glycogen storage. On the mechanism, we screened and identified that glycogen synthase 2 (Gys2) plays a critical role in m6A-mediated regulation of liver glycogen storage. Furthermore, IGF2BP2, as a “reader” of m6A, stabilizes the mRNA of Gys2. More importantly, reconstitution of GYS2 rescues liver glycogenesis in Mettl3-cKO mice. Collectively, a METTL3-IGF2BP2-GYS2 axis, in which METTL3 and IGF2BP2 regulate glycogenesis as “writer” and “reader” respectively, plays a critical role on maintenance of liver glycogenesis in mammals.

Introduction

Hepatic glycogen maintains the blood glucose concentration between meals. In humans, defects in glycogenesis cause different types of glycogen storage diseases, which may lead to failure to thrive in some pediatric patients [1,2]. Intriguingly, under physiological conditions, the hepatic glycogen content increases gradually from birth to adulthood in numerous mammals, such as rats, rabbits, sheep, and rhesus macaques[3–5]. And the blood glucose concentration has a similar pattern [6]. However, the detailed mechanism and biological meaning of this phenomenon remain unclear.

Among the more than one hundred RNA modifications, N6-methyladenosine (m6A) was identified in the 1970s[7]. M6A is the most abundant modification in eukaryotic mRNAs[8] and functions as an epitranscriptomic regulator of target mRNAs through multiple mechanisms, including regulating mRNA stability and translation efficiency [9]. As early as in 1990s, MT-A70, also known as Mettl3 this years, was reported having methyltransferases activity of m6A[10]. However, approximately a decade ago, the identification of the first RNA demethylase, fat mass and obesity-associated protein (FTO), revealed that N6-methyladenosine modification is reversible[11]. And consequently, a methyltransferase complex consisting mainly of methyltransferase-like 3 (METTL3), methyltransferase-like 14 (METTL14) and Wilmstumor-associated protein (WTAP) has been proven to act as an m6A methyltransferase (“writer”) in mammalian cells[12,13]. Same as previously reported, METTL3 is the essential catalytic component of the complex[14–18]. Then, a group of YT521-B homology (YTH) domain-containing family proteins (YTHDFs) have been identified as m6A “readers” that control mRNA fate by regulating pre-mRNA splicing, facilitating mRNA translation or promoting mRNA decay[19–25]. Strikingly, in a recent report Huang et al demonstrated that insulin-like growth factor 2 (IGF2) mRNA-binding proteins 1, 2 and 3 (IGF2BP1/2/3) preferentially recognized m6A-modified mRNAs and promoted the stability (and likely the translation) of thousands of potential target mRNAs in an m6A-dependent manner, thereby affecting global gene expression output[26].

Importantly, with deeply understanding the biochemical process of N6-methyladenosine modification in the past decade, more studies has moved forward to explore the functional significance of m6A in various biological processes, including DNA damage repair [27], meiosis [28], circadian clock [29] and tumor immune surveillance[30]. Transcriptome-wide mapping of m6A modification has revealed cell type-specific methylation targets, suggesting that m6A regulates cell type-specific processes[31]. Liver is an important metabolic organ in the body, and maintaining its functional homeostasis is essential for health. It was reported that inhibition of m6A methylation decreases the m6A abundance in PPaRα and increases the lifetime and expression of PPaRα mRNA, reducing lipid accumulation in hepatocytes[32]. In addition, m6A modification can also orchestrate sex-dimorphic metabolic traits in liver. Loss of m6A control in male livers increases hepatic triglyceride stores, leading to a more 'feminized' hepatic lipid composition[33]. All the evidence supports that dynamic modification of m6A is essential for the multiple functions of liver tissues.

In the present study, we found a significant increase in the m6A level in the hepatocytes of growing mice. Strikingly, hepatic glycogen was almost completely absent in mice with liver-specific *Mettl3* deletion. Analysis of m6A sequencing (m6A-seq) and m6A-methylated RNA immunoprecipitation sequencing with qRT-PCR (MeRIP-qPCR) showed that METTL3 induced an increase in the m6A level in *Gys2* mRNA and promoted IGF2BP2-mediated *Gys2* mRNA stability. Importantly, reintroduction of exogenous GYS2 partially rescued glycogen storage in *Mettl3*-deficient hepatocytes *in vivo*. Furthermore, co-expression of *Mettl3* and *Gys2* is associated with liver glycogen storage in other mammals, such as Sprague-Dawley rats. Taken together, Our study revealed that a METTL3-IGF2BP2-GYS2 axis potentially regulates the hepatic glycogen quantity.

Results

N6-methyladenosine modification is related to the shortage of hepatic glycogen in mouse pups.

Mice are usually weaned after 4 weeks of age and reach sexual maturity between 6 and 8 weeks. After 8 weeks of age, most mice have the ability to procreate. Here, we measured liver glycogen levels in C57BL/6 mice in a free diet at different ages and found that glycogen storage in the liver gradually increased with the growth of mice (Figure 1a). Via transmission electron microscopy (TEM), only a few glycogen molecules were observed in hepatocytes from 4-week-old mice; however, hepatocytes from 8-week-old mice contained an abundance of glycogen in the cytoplasm (Figure 1b). Intriguingly, the m6A/A ratio in livers' RNAs that contain poly(A) tails had a similar pattern to that of glycogen storage at the indicated ages (Figure 1c).

Mettl3 depletion simulates lack of glycogen in liver.

To verify whether m6A modification plays a key role in liver glycogen storage, we generated a hepatocyte-specific *Mettl3* knockout model, albumin-Cre *Mettl3*$^{fl/fl}$ (Supplementary Figure 1). As expected, the decline in the m6A/A ratio was observed in cKO-mice's liver tissue RNAs (Supplementary Figure 1c). Periodic

acid-Schiff (PAS) staining revealed that glycogen shortage in the liver was simulated in *Mettl3*-conditional knockout (cKO) mouse (Figure 2a). Via transmission electron microscopy, almost no glycogen could be observed in hepatocytes of *Mettl3*-cKO mice (Figure 2b). In addition, AQP8, a channel protein that was reported to have a close temporal and spatial correlation with glycogen accumulation in hepatocytes [34], was downregulated in *Mettl3*-cKO mice (Supplementary Figure 1e). Considering that the most important function of liver glycogen is blood glucose maintenance, we measured the serum glucose level in mice of different genotypes and found that it was greatly reduced in *Mettl3*-cKO mice (Figure 2c). Furthermore, *Mettl3*-cKO mice also had worse performance than wild-type (WT) and heterogeneous(HET) mice in the forced swim test (Figure 2d).

Identification of Gys2 mRNA by global N6-methyladenosine modification analysis as a key substrate of METTL3 in mouse liver glycogenesis

To investigate the role of m6A in liver glycogen storage, total RNA was isolated from samples of *Mettl3*-WT and *Mettl3*-cKO liver tissue for m6A profiling by MeRIP-seq. Motif searching identified the consensus "GGACU" motif within the m6A sites (Figure 3a). The density of m6A peaks increased steadily along the transcript in the CDS and decreased along the 3'-UTR (Figure 3b). Gene Ontology (GO) terms related to numerous metabolic processes were the most significantly enriched with genes exhibiting m6A peak loss (Figure 3c) and downregulated expression (Figure 3d) in *Mettl3*-cKO liver tissue. These results suggested that m6A modification has a considerable influence on metabolic pathways. Then, we obtained 26 candidate genes from one MeRIP-seq dataset and three independent RNA sequencing (RNA-seq) datasets. All 26 genes exhibited both m6A peak loss and a pattern of downregulated expression (Figure 3e, left). Among these 26 genes was fatty acid synthase (Fasn), which was reported to be a substrate of METTL3 in hepatocytes[35]. Intriguingly, this gene set contained glycogen synthase 2 (*Gys2*), the key enzyme coding gene of glycogenesis in liver (Figure 3e right).

In addition, MeRIP-qPCR confirmed that *Gys2* mRNA was an m6A-regulated target (Figure 3f). m6A MeRIP-Seq revealed that *Gys2* has highly enriched and specific m6A peaks among its coding sequence and near its translation stop codon, but these peaks almost lost in *Mettl3*-cKO liver tissue (Figure 3g). Furthermore, much lower *Gys2* expression at both the mRNA (Figure 3h) and protein (Figure 3i) levels were found in livers of *Mettl3*-cKO mice.

Taken together, *Gys2*, the key enzyme of glycogenesis in hepatocytes, is a candidate target of METTL3 in liver. And loss of m6A modifications of *Gys2* mRNA perish its expression both in RNA and protein levels.

N6-methyladenosine stabilizes Gys2 mRNA in an IGF2BP2-dependent manner.

Different functions of m6A modification are reported to be mediated by different m6A binding proteins (i.e.,readers), such as YTHDF1/2/3 and IGF2BP1/2/3 [36]. As shown in Figure 3h, the *Gys2* mRNA level was much lower in liver tissue in *Mettl3*-cKO mice than in control mice. Therefore, we focused on five readers that are known to enhance the stabilization of mRNAs in the cytoplasm or mediate their nucleocytoplasmic trafficking [36]. To determine which reader mediate the mRNA stability of *Gys2*, we first

determined *Gys2* expression level in seven liver-associated cell lines and HEK-293T cells. Surprisingly, *Gys2* had the highest expression level in HEK-293T cells (Supplementary Figure 2a). Then, we independently depleted the five candidate readers in HEK-293T cells and found that depletion of only IGF2BP2 reduced *Gys2* mRNA expression (Figure 4a, Supplementary Figure 2b-f). Furthermore, we used more siRNAs to independently deplete IGF2BP2 and found that *Gys2* mRNA expression followed a pattern similar to IGF2BP2 expression (Figure 4b). In addition, mRNA decay assays demonstrated that a reduction in IGF2BP2 expression appreciably promoted the decay of *Gys2* mRNA (Figure 4c). Finally, RNA Immunoprecipitation (RIP) assays revealed the binding between IGF2BP2 protein and *Gys2* mRNA (Figure 4d).

To confirm that *Gys2* expression is regulated by IGF2BP2 in an m6A-dependent manner, we analyzed the conserved m6A motifs in *Gys2* among multiple mammals, including humans and mice, and then mutated the highly conserved m6A motif GGACU to GCUCU (Gys2-CDS Mut) (Figure 4e). After transient transfection of Gys2-CDS WT or Gys2-CDS Mut into HEK-293T cells, exogenous GYS2 expression was almost completely abolished in Gys2-CDS Mut cells, indicating that regulation of *Gys2* expression is mediated mainly through this m6A motif (Figure 4f). In addition, knockdown of IGF2BP2 reduced the level of exogenous GYS2 (Figure 4f). Taken together, these findings indicated that *Gys2* mRNA is a bona fide substrate of METTL3 and that *Gys2* mRNA is stabilized by IGF2BP2 in an m6A-dependent manner.

Reconstitution of GYS2 rescues liver glycogenesis in Mettl3-cKO mice.

To verify the METTL3-IGF2BP2-GYS2 axis, we reconstituted the activation of GYS2 in the *Mettl3*-cKO mouse livers via adeno-associated virus (AAV)-mediated transduction. Compared to control AAV (AAV-luciferase, AAV-Luc), AAV-Gys2 restored the GYS2 protein level in *Mettl3*-cKO mice to the baseline level (Figure 5a-c). PAS staining (Figure 5d) and transmission electron microscopy (Figure 5e) revealed that reconstitution of GYS2 activation partially restored liver glycogen storage in *Mettl3*-cKO mice. Systemically, both the serum glucose level in *Mettl3*-cKO mice in a free diet (Figure 5f) and the blood glucose level in *Mettl3*-cKO mice after prolonged fasting (Figure 5g) were increased under AAV-Gys2 treatment. In addition, *Mettl3*-cKO mice with AAV-Gys2 intervention performed better in the forced swim test than *Mettl3*-cKO mice with AAV-Luc intervention, although a performance gap remained between these mice and HET mice (Figure 5h). In summary, reconstitution of GYS2 activation reversed *Mettl3*-cKO-associated glycogen deficiency and the related phenotypes in mice.

The METTL3-IGF2BP2-GYS2 axis is related to liver glycogen storage in rats.

Liver glycogen storage is very important for almost all mammals. To investigate whether the axis we found in mouse exist in other mammals, we test the samples from Sprague-Dawley (SD) rats. First, Periodic acid-Schiff (PAS) staining revealed that glycogen shortage in the liver is much lower in 4-week-old male rats than 8-week-old ones (Figure 6a). It suggested that, similar to mouse, adult rats also have high level glycogen in liver comparing to pups. In addition, the m6A/A ratio in livers' RNAs that contain poly(A) tails had a similar pattern to that of glycogen storage at the indicated ages (Figure 6b). Furthermore, qRT-PCR assay demonstrated that mRNA of *Mettl3* (Figure 6c), *Igf2bp2* (Figure 6d) and

Gys2 (Figure 6e) in livers are higher in 8-week-old rats and lower in 4-week-old rats. Finally, we tested serum glucose of different age rats in free diet. As expected, 8-week-old rats have higher serum glucose than 4-week-old ones (Figure 6f). Taken together, these results suggest that the METTL3-IGF2BP2-GYS2 axis we found in mouse may also exist in other mammals, such as rats.

Discussion

Under physiological conditions, human blood should contain only 4 to 6 grams of glucose, but the daily consumption of glucose for a normal person is approximately 160 grams [37]. Glycogen synthesis and breakdown in the liver maintain the homeostasis of blood glucose between meals, and disorders of liver glycogen metabolism often cause severe outcomes and even death in some pediatric patients [1,2]. Previous articles and our data (Figure 1a-b, Figure 6a) revealed that the concentration of glycogen in the liver increases gradually from birth to adulthood in numerous mammals, such as mice, rats, rabbits, sheep, and rhesus macaques [3–5, 34].The blood glucose level exhibits a similar pattern [6]. However, the detailed mechanism and biological meaningof this phenomenon remain unclear.

Among the more than one hundred mRNA modifications, N6-methyladenosine (m6A) was identified in the 1970s[7]. M6A modification is the most abundant modification in eukaryotic mRNAs[8] and functions as an epitranscriptomic regulator of target mRNAs through multiple mechanisms, including enhancing stability and translation efficiency[9]. Intriguingly, we found that the m6A/A ratio in RNAs that contain poly(A) tails had a pattern similar to the glycogen storage at the indicated ages (Figure 1c). It suggested that m6A modification of mRNA might be involved in glycogen metabolism.

Approximately a decade ago, an important report identified the first RNA demethylase (m6A “eraser”), fat mass and obesity-associated protein (FTO), revealing that RNA modification is reversible [11]. Then, ALKBH5 was confirmed as another m6A eraser in mammals[38]. On the other hand, m6A methyltransferases (“writers”) in mammalian cells are complexes that contain various protein components. Methyltransferase-like 3 (METTL3) and methyltransferase-like 14 (METTL14) are still the core methyltransferases, although an increasing number of subunits have been verified[36]. Here, to reveal whether m6A modification plays a key role in glycogen storage, we generated a hepatocyte-specific *Mettl3* knockout model (Albumin-Cre*Mettl3*$^{fl/fl}$). As expected, the m6A/A ratio in RNAs that contain poly(A) tails reduced in conditional knockout (cKO) mouse livers (Supplementary Figure 1c). In addition, *Mettl3* depletion simulated lack of glycogen in livers (Figure 2a-b and Supplementary Figure 1e). Furthermore, liver-specific depletion of *Mettl3* in mice resulted in hypoglycemia under free diet conditions (Figure 2c) and poor performance in the forced swim test (Figure 2d).

To identify substrates of METTL3 in the liver, we extracted total RNA from tissues at the same anatomic site from wild-type (WT) and conditional knockout (cKO) mice. MeRIP-seq and RNA-seq revealed that numerous metabolic processes were dysregulated (Figure 3c-d), suggesting that the principal difference in this model was established. Then, we focused on 26 candidate genes that exhibited both m6A peak

loss and a pattern of down-regulated expression in the livers of *Mettl3*-cKO mice. *Fasn*, a previously reported substrate of METTL3 in the mouse liver [35], was included in this 26-gene set (Figure 3e right). Intriguingly, this gene set also contained glycogen synthase 2 (*Gys2*), the key enzyme coding gene of glycogenesis in liver (Figure 3e right). MeRIP-qPCR and meRIP-seq peaks revealed the presence of m6A modification in *Gys2* mRNA (Figure 3f-g). Furthermore, the construct with mutation of the potential binding site in the *Gys2* CDS retained a much lower expression level than the WT construct (Figure 4e-f). Taken together, these results indicated that *Gys2* mRNA is a bona fide substrate of METTL3 in the mouse liver.

Similar to the functions of other epigenetic modifications, the functions of RNA m6A modification are carried out by RNA binding proteins called m6A readers. Previously, a group of YT521-B homology (YTH) domain-containing family proteins (YTHDFs) were identified as m6A readers that control mRNA fate by regulating pre-mRNA splicing, facilitating mRNA translation or promoting mRNA decay[19–23]. Later, an increasing number of readers, including hnRNPA2B1 and HuR, were identified [36]. Among these readers, insulin-like growth factor 2 (IGF2) mRNA-binding proteins 1, 2 and 3 (IGF2BP1/2/3) were reported by Huang et al to preferentially recognize m6A-modified mRNAs and promote the stability (and probably also the translation) of thousands of potential mRNA targets in an m6A-dependent manner, thereby affecting global gene expression output [26]. Therefore, readers can be classified into various types in accordance with their function in m6A modification[36]. In this study, a striking effect of *Mettl3* depletion was a substantially diminished *Gys2* mRNA level (Figure 3h); thus, we focused on readers that can stabilize or mediate the nucleocytoplasmic trafficking of target mRNAs [36]. IGF2BP2 but not the other four candidate genes (IGF2BP1/3, hnRNPA2B1 and HuR) bound and stabilized *Gys2* mRNA in cells (Figure 4).

Logically, if the METTL3-IGF2BP2-GYS2 axis exists in cells, reconstitution of GYS2 activation would be expected to rescue *Mettl3*-cKO-associated hepatic glycogen deficiency. Here, reconstitution of GYS2 in hepatocytes of *Mettl3*-cKO mice by adeno-associated virus (AAV)-mediated transduction partially enhanced the accumulation of glycogen in the liver (Figure 5d-e), improved serum glucose in free diet-fed mice (Figure 5f), and increased blood glucose in mice after prolonged fasting (Figure 5g). Moreover, the performance of *Mettl3*-cKO mice in the forced swim test was enhanced under AAV-GYS2 intervention (Figure 5h). In conclusion, reconstitution of GYS2 activation rescued the unfavorable phenotypes associated with *Mettl3*-cKO in mice.

However, all the results we obtained above were from mice. Do other mammals, such as rats, also have this phenomenon? In order to answer this question, we investigated samples from male rats in different ages, and found that adult rats really have more glycogen storage than pups (Figure 6a). As expected, the m6A/A ratios of mRNA in livers have similar patterns to glycogen storage in indicated ages (Figure 6b). Furthermore, *Mettl3*, *Igf2bp2* and *Gys2* also have much higher expression in livers of adult rats (Figure 6c-e). In addition, serum glucose of 8-week-old rats are higher than that of 4-week-old ones (Figure 6f). Taken together, our results suggested that the phenomenon and mechanism, we found in mice, could also exist in other mammals, such as rats.

In summary, we revealed a METTL3-IGF2BP2-GYS2 axis that controlled glycogenesis in mammalian liver. On the one hand, this axis limited liver glycogen storage in mammalian pups to a very low level. As a result, a lack of glycogen in the liver could improve the safety of animal pups in the wild by necessitating a short interval between feedings by their parents. On the other hand, this axis increases liver glycogen storage in adult mammals. Interestingly, under this condition, the abundance of glycogen in the liver could also improve the safety and facilitate the survival of adult mammals by allowing a long interval between meals in the wild (Figure 7).

Materials And Methods

Mice

Methyltransferase-like 3 (Mettl3)-floxed mice were generated by Beijing Biocytogen Co., Ltd. Alb-Cre mice purchased from The Jackson Laboratory were crossed with Mettl3-floxed mice to generate Alb-cre Mettl3$^{-/-}$ (wild-type, WT), Alb-cre Mettl3$^{fl/-}$ (HET) and Alb-cre Mettl3$^{fl/fl}$ (KO) mice. The PCR primers used for genotyping of each mouse strain are listed in Supplemental Table S1. Without special instructions, experimental mice were bred and maintained under specific pathogen-free conditions, fed standard laboratory chow, and kept on a 12h light/dark cycle. All mice were on the C57BL/6 genetic background and were housed in individual cages. Littermate KO mice were used as the control animals in each experiment. All animal experiments were approved by the Animal Experiment Administration Committee of the Fourth Military Medical University.

Rats

Experimental Sprague-Dawley (SD) rats were purchased from Lab Animal Center of the Fourth Military Medical University. SD Rats were bred and maintained under specific pathogen-free conditions, fed standard laboratory chow, and kept on a 12h light/dark cycle. All animal experiments were approved by the Animal Experiment Administration Committee of the Fourth Military Medical University.

Animal studies

Serum glucose detection (mice): Normal diet-fed mice with the indicated genotypes (8-week-old male mice, n≥5) were sacrificed.Total blood was collected and centrifuged (1500 g/min, 5 min) to isolate serum. The serum glucose level was measured by Servicebio, Inc.

Serum glucose detection (rats): Normal diet-fed rats with the indicated ages (male, n≥5) were sacrificed. Total blood was collected and centrifuged (1500 g/min, 5 min) to isolate serum. The serum glucose level was measured by Servicebio, Inc.

Blood glucose detection: Mice with the indicated genotypes (8-week-old male mice, n≥5) fasted for 12-24 h. Blood glucose was measured using blood collected from mouse tail veins under sedation.

Forced swim test: Mice with the indicated genotypes (8-week-old male mice, n≥5) were tested with a method based on a previous report [39].

Adeno-associated virus (AAV)-mediated reconstitution of liver-specific glycogen synthase (Gys2) activation: AAVs containing luciferase (Luc) or Gys2 constructs were injected i.v.into mice with the indicated genotypes (8-week-old male mice, n≥6). Three weeks after injection, mice were evaluated by the indicated assays.

Cell culture

An immortalized human hepatocyte cell line (L-02) and human liver cancer cell lines (BEL-7404, HepG2, SMMC-7721, Huh7, Hep3B and PLC/PRF/5) were obtained from the Type Culture Collection of the Chinese Academy of Sciences, as was thehuman embryonic kidney cell line HEK-293T.

HEK-293T, HepG2 and PLC/PRF/5 cell lines were maintained in Dulbecco's modified Eagle's medium (DMEM; Gibco BRL, USA) supplemented with 10% fetal calf serum (FCS; Gibco BRL, USA), 2 mM L-glutamine and antibiotics (complete medium). Huh7, SMMC-7721, L-02 and BEL-7404 cell lines were maintained in Roswell Park Memorial Institute (RPMI)-1640 medium (Gibco BRL, USA) supplemented with 10% FCS and antibiotics. Hep3B cells were maintained in minimal essential medium (MEM; Invitrogen, USA) supplemented with 10% FCS and antibiotics. All cell lines were incubated in a humidified atmosphere of 5% CO_2 in air at 37°C.

AAV vector production

Recombinant AAV vectors were produced by a standard triple-transfection calcium phosphate precipitation method using AAV-293 cells. The production plasmids (AAV-MCS, AAV-DJ and pHelper) were from the AAV-DJ Helper Free Expression System (CELL BIOLABS, VPK-410-DJ), and the AAV-Luc and AAV-Gys2 constructs were generated from AAV-MCS. Purification was performed with clarified AAV-293 cell lysates using a ViraBind™ AAV Purification Mega Kit (CELL BIOLABS, VPK-141). Viral genome (vg) titers were determined with a QuickTiter™ AAV Quantitation Kit (CELL BIOLABS, VPK-145).

Glycogen quantification and histological detection

Qualitative assessment of liver tissue glycogen was performed using periodic acid-Schiff (PAS) staining. Mice/rats with the indicated genotypes or ages (n≥5) were sacrificed. The livers were rapidly harvested, and slices of the left and medial lobes were obtained and post fixed overnight with 4% paraformaldehyde in phosphate-buffered saline. Liver tissues were embedded in paraffin, sectioned (4 μm), and stained with PAS following the protocol of Vesselinovitch et al[40]. Immunohistochemical assays were performed on FFPE sections as reported previously [41]. Antibodies against Gys2 (1:100, 22371-1-AP, Proteintech®) were used. Staining intensities were measured using ImageJ software (National Institutes of Health, Bethesda, MD, USA).

Transmission electronmicroscopy(TEM)

Liver samples were obtained from the left lobe and were fixed with 2.5% glutaraldehyde (pH = 7.2) and 1% osmium tetroxide and processed as described previously[42].The slices were examined with a transmission electron microscope (JEM-1230, JEOL Ltd., Tokyo, Japan). Images were acquired by a technician blinded to the treatment.

Quantitative real-time PCR (qRT-PCR)

Total RNA was isolated from cells using TRIzol (Invitrogen). For qRT-PCR analysis of mRNAs, first-strand cDNA was synthesized using a Prime Script qRT-PCR Kit (Takara). The expression levels of the target genes were determined by amplification with specific primers. The primers used are listed in Table S2.

N6-methyladenosine (m6A)-sequencing (m6A-seq) and quantification of mRNA methylation by m6A-methylated RNA immunoprecipitation sequencing with RT-qPCR (MeRIP-qPCR)

Total RNA was isolated from cells using TRIzol (Invitrogen). Then, m6A-seq was performed (CloudSeq Biotech, Shanghai, China). For MeRIP-qPCR, poly(A)$^+$ mRNA was isolated using a Dynabeads^{TM} mRNA Direct Purification Kit (61006, Invitrogen). Purified RNA (2 μg) was used for enrichment of m6A-containing mRNA with a Magna MeRIP^{TM} m^{6}A Kit (17-10499-1, Millipore), and the RNA was purified according to the manufacturer's protocol. The resulting final product was used for qRT-PCR. The primers used to amplify mouse Gys2 mRNA are listed in Table S2.

Quantification of RNA methylation

mRNA was isolated using the Dynabeads^{TM} mRNA Direct Purification Kit (61006, Invitrogen). Methylation of purified mRNA was quantified using an EpiQuik m6A RNA Methylation Quantification Kit (P-9005, EpiGentek) according to the manufacturer's protocol.

RNA immunoprecipitation-qPCR (RIP-qPCR)

This procedure was performed according to a previously published report[26]. HEK-293T cells were washed twice with PBS and lysed in lysis buffer (150 mMKCl, 10 mM HEPES (pH 7.6), 2 mM EDTA, 0.5% NP-40, 0.5 mM dithiothreitol (DTT), 1:100 protease inhibitor cocktail, 400 U/ml RNase inhibitor). The cell lysates were centrifuged. A 50-μl aliquot of the cell lysate was saved as input, and the remaining sample was incubated with 20 μl of protein A beads previously bound to IgG or an anti-insulin-like growth factor 2 mRNA-binding protein 2 (IGF2BP2) antibody (Proteintech^{TM}) for 4 h at 4 °C. The beads were washed 2 times with wash buffer (50 mMTris, 200mMNaCl, 2 mM EDTA, 0.05% NP40, 0.5mM DTT, RNase inhibitor). RNA was eluted from the beads with 50 μl of RLT buffer and purified with RNeasy columns (217004, QIAGEN). RNA was eluted in 100 μl of RNase-free water and reverse transcribed into cDNA using a Prime Script qRT-PCR Kit (Takara) according to the manufacturer's instructions. The fold enrichment was determined by qRT-PCR. The primers used for amplifying human Gys2 mRNA are listed in Table S2.

mRNA stability analysis

To evaluate mRNA stability, HEK-293T cells were treated with actinomycin D (Sigma) at a final concentration of 5μg/ml for 0, 2, or 4 h. The cells were collected, and RNA samples were extracted for reverse transcription. The mRNA transcript levels of interest were determined by qRT-PCR.

Western blot analysis

Cells were harvested and lysed with RIPA buffer. The protein concentration was determined using a BCA kit. Samples were separated on 10% SDS-PAGE gels and blotted onto nitrocellulose membranes (Millipore). Membranes were incubated at 4 °C overnight with primary antibodies at the following concentrations: anti-GYS2 (1:2000, 22371-1-AP, Proteintech®), anti-METTL3 (1:1000, 18810, Abcam), and anti-β-actin (1:5000, Sigma). Membranes were then washed three times with TBST and incubated with HRP-conjugated anti-mouse IgG (1:10000, 7076, Cell Signaling Technology) or anti-rabbit IgG (1:10000, 7074, Cell Signaling Technology) diluted in TBST containing 1% non-fat milk at room temperature for 1 h. After a final wash with TBST, the membranes were developed with ECL reagents and visualized using a Tanon 5500 imaging system. The ratio of the expression of the indicated molecule to that of β-actin was determined using ImageJ software (National Institutes of Health, Bethesda, MD, USA).

Bioinformatic analysis

Figure 3a-b: Motif analysis was performed using HOMER [43] to search motifs in each set of m6A peaks. Metagene profiles were generated as described [19]. Figure 3c-d: Gene Ontology (GO) biological process (BP) enrichment was analyzed by CloudSeq Biotech; $p < 0.05$ was considered to indicate significant enrichment.

Statistical analysis

Data were analyzed using SPSS software. For experiments including analysis of the positive staining area, qRT-PCR, MeRIP-qPCR, forced swim tests, or glucose level detection, statistical significance was evaluated using two-tailed Student's t-test, with $P < 0.05$ considered significant.

Declarations

Competing interests

The authors declare no competing interests.

Acknowledgments

This work was supported by grants from the National Natural Science Foundation of China (81630069, 81421003 and 31771439 to A.G.Y.; 81773262, 81572763 and 82173046 to R.Z.; 82173162 to X.Z.; 31801128 to H.L.Y.); the Grant of Youth Training Project of PLA Medical Science and Technology, China (18QNP018 to X.Z.); the Key Research and Development Project of Shaanxi Province (2020SF-137 to X.Z.); and the Fund of State Key Laboratory of Cancer Biology (CBSKL2015Z15 to X.Z.).

Author contributions

Conceptualization: X.Z. and R.Z.; Methodology: X.Z., H.Y. and Xiaofang Z.; Investigation: X.Z., H.Y, Y.P., D.L., Y.Y., J.Z., X.J., S.C., Y.L. and Xiaofang Z.; Writing – Original Draft: X.Z. and R.Z.; Writing – Review & Editing: X.Z. and R.Z.; Funding Acquisition: X.Z., R.Z., H.Y. and A.Y.; Resources: X.Z. and R.Z.; Supervision: R.Z.

Data availability

All data generated or analysed during this study are included in this article and its supplementary files. Sequencing data have been submitted to NCBI/GEO (GSE185142, secure token for reviewers: kjmluiokfngxpgl). Source data are provided with this paper.

References

1 Orho, M. *et al.* Mutations in the liver glycogen synthase gene in children with hypoglycemia due to glycogen storage disease type 0. *The Journal of clinical investigation* **102**, 507-515, doi:10.1172/JCI2890 (1998).

2 Bao, Y., Kishnani, P., Wu, J. Y. & Chen, Y. T. Hepatic and neuromuscular forms of glycogen storage disease type IV caused by mutations in the same glycogen-branching enzyme gene. *The Journal of clinical investigation* **97**, 941-948, doi:10.1172/JCI118517 (1996).

3 HJ, S. GLYCOGEN RFSERVES AND THEIR CHANGES AT BIRTH AND IN ANOXIA. *British Medical Bulletin* **17**, 137-143, doi:doi.org/10.1093/oxfordjournals.bmb.a069888 (1961).

4 Bhavnani, B. R. Ontogeny of some enzymes of glycogen metabolism in rabbit fetal heart, lungs, and liver. *Canadian journal of biochemistry and cell biology = Revue canadienne de biochimie et biologie cellulaire* **61**, 191-197, doi:10.1139/o83-027 (1983).

5 Bohme, H. J., Sparmann, G. & Hofmann, E. Biochemistry of liver development in the perinatal period. *Experientia* **39**, 473-483, doi:10.1007/BF01965164 (1983).

6 Shelley, H. J. & Neligan, G. A. Neonatal hypoglycaemia. *Br Med Bull* **22**, 34-39, doi:10.1093/oxfordjournals.bmb.a070433 (1966).

7 Perry, R. P. & Kelley, D. E. Existence of methylated messenger RNA in mouse L cells. *Cell* **1**, 37-42, doi:10.1016/0092-8674(74)90153-6 (1974).

8 Machnicka, M. A. *et al.* MODOMICS: a database of RNA modification pathways–2013 update. *Nucleic acids research* **41**, D262-267, doi:10.1093/nar/gks1007 (2013).

9 Meyer, K. D. & Jaffrey, S. R. The dynamic epitranscriptome: N6-methyladenosine and gene expression control. *Nature reviews. Molecular cell biology* **15**, 313-326, doi:10.1038/nrm3785 (2014).

10 Bokar, J., Shambaugh, M., Polayes, D., Matera, A. & Rottman, F. Purification and cDNA cloning of the AdoMet-binding subunit of the human mRNA (N6-adenosine)-methyltransferase. *RNA (New York, N.Y.)* **3**, 1233-1247 (1997).

11 Jia, G. *et al.* N6-methyladenosine in nuclear RNA is a major substrate of the obesity-associated FTO. *Nature chemical biology* **7**, 885-887, doi:10.1038/nchembio.687 (2011).

12 Liu, J. *et al.* A METTL3-METTL14 complex mediates mammalian nuclear RNA N6-adenosine methylation. *Nature chemical biology* **10**, 93-95, doi:10.1038/nchembio.1432 (2014).

13 Ping, X. L. *et al.* Mammalian WTAP is a regulatory subunit of the RNA N6-methyladenosine methyltransferase. *Cell research* **24**, 177-189, doi:10.1038/cr.2014.3 (2014).

14 Geula, S. *et al.* Stem cells. m6A mRNA methylation facilitates resolution of naive pluripotency toward differentiation. *Science* **347**, 1002-1006, doi:10.1126/science.1261417 (2015).

15 Sledz, P. & Jinek, M. Structural insights into the molecular mechanism of the m(6)A writer complex. *eLife* **5**, doi:10.7554/eLife.18434 (2016).

16 Wang, P., Doxtader, K. A. & Nam, Y. Structural Basis for Cooperative Function of Mettl3 and Mettl14 Methyltransferases. *Molecular cell* **63**, 306-317, doi:10.1016/j.molcel.2016.05.041 (2016).

17 Wang, X. *et al.* Structural basis of N(6)-adenosine methylation by the METTL3-METTL14 complex. *Nature* **534**, 575-578, doi:10.1038/nature18298 (2016).

18 Ramalingam, H. *et al.* A methionine-Mettl3-N-methyladenosine axis promotes polycystic kidney disease. *Cell metabolism* **33**, 1234-1247.e1237, doi:10.1016/j.cmet.2021.03.024 (2021).

19 Dominissini, D. *et al.* Topology of the human and mouse m6A RNA methylomes revealed by m6A-seq. *Nature* **485**, 201-206, doi:10.1038/nature11112 (2012).

20 Wang, X. *et al.* N6-methyladenosine-dependent regulation of messenger RNA stability. *Nature* **505**, 117-120, doi:10.1038/nature12730 (2014).

21 Wang, X. *et al.* N(6)-methyladenosine Modulates Messenger RNA Translation Efficiency. *Cell* **161**, 1388-1399, doi:10.1016/j.cell.2015.05.014 (2015).

22 Du, H. *et al.* YTHDF2 destabilizes m(6)A-containing RNA through direct recruitment of the CCR4-NOT deadenylase complex. *Nature communications* **7**, 12626, doi:10.1038/ncomms12626 (2016).

23 Xiao, W. *et al.* Nuclear m(6)A Reader YTHDC1 Regulates mRNA Splicing. *Molecular cell* **61**, 507-519, doi:10.1016/j.molcel.2016.01.012 (2016).

24 Zaccara, S. & Jaffrey, S. A Unified Model for the Function of YTHDF Proteins in Regulating mA-Modified mRNA. *Cell* **181**, 1582-1595.e1518, doi:10.1016/j.cell.2020.05.012 (2020).

25 Dixit, D. *et al.* The RNA m6A Reader YTHDF2 Maintains Oncogene Expression and Is a Targetable Dependency in Glioblastoma Stem Cells. *Cancer discovery* **11**, 480-499, doi:10.1158/2159-8290.cd-20-0331 (2021).

26 Huang, H. *et al.* Recognition of RNA N(6)-methyladenosine by IGF2BP proteins enhances mRNA stability and translation. *Nature cell biology* **20**, 285-295, doi:10.1038/s41556-018-0045-z (2018).

27 Xiang, Y. *et al.* RNA m(6)A methylation regulates the ultraviolet-induced DNA damage response. *Nature* **543**, 573-576, doi:10.1038/nature21671 (2017).

28 Agarwala, S. D., Blitzblau, H. G., Hochwagen, A. & Fink, G. R. RNA methylation by the MIS complex regulates a cell fate decision in yeast. *PLoS genetics* **8**, e1002732, doi:10.1371/journal.pgen.1002732 (2012).

29 Fustin, J. M. *et al.* RNA-methylation-dependent RNA processing controls the speed of the circadian clock. *Cell* **155**, 793-806, doi:10.1016/j.cell.2013.10.026 (2013).

30 Liu, Y. *et al.* Tumors exploit FTO-mediated regulation of glycolytic metabolism to evade immune surveillance. *Cell metabolism* **33**, 1221-1233.e1211, doi:10.1016/j.cmet.2021.04.001 (2021).

31 Chen, T. *et al.* m(6)A RNA methylation is regulated by microRNAs and promotes reprogramming to pluripotency. *Cell stem cell* **16**, 289-301, doi:10.1016/j.stem.2015.01.016 (2015).

32 Zhong, X. *et al.* Circadian Clock Regulation of Hepatic Lipid Metabolism by Modulation of m(6)A mRNA Methylation. *Cell reports* **25**, 1816-1828 e1814, doi:10.1016/j.celrep.2018.10.068 (2018).

33 Salisbury, D. A. *et al.* Transcriptional regulation of N-6-methyladenosine orchestrates sex-dimorphic metabolic traits. *Nat Metab* **3**, 940-+, doi:10.1038/s42255-021-00427-2 (2021).

34 Ferri, D. *et al.* Ontogeny, distribution, and possible functional implications of an unusual aquaporin, AQP8, in mouse liver. *Hepatology (Baltimore, Md.)* **38**, 947-957, doi:10.1053/jhep.2003.50397 (2003).

35 Xie, W., Ma, L. L., Xu, Y. Q., Wang, B. H. & Li, S. M. METTL3 inhibits hepatic insulin sensitivity via N6-methyladenosine modification of Fasn mRNA and promoting fatty acid metabolism. *Biochem Bioph Res Co* **518**, 120-126, doi:10.1016/j.bbrc.2019.08.018 (2019).

36 Liang, W. C., Lin, Z. X., Du, C., Qiu, D. B. & Zhang, Q. mRNA modification orchestrates cancer stem cell fate decisions. *Mol Cancer* **19**, doi:Artn 38 10.1186/S12943-020-01166-W (2020).

37 Rodwell, V. W., Bender, D.A., Botham,K.M., Kennelly, P.J., Weil, P.A. volumes (Lange Medical Books/McGraw-Hill, New York, 2015).

38 Zheng, G. *et al.* ALKBH5 is a mammalian RNA demethylase that impacts RNA metabolism and mouse fertility. *Molecular cell* **49**, 18-29, doi:10.1016/j.molcel.2012.10.015 (2013).

39 McArdle, W. D. & Montoye, H. J. Reliability of exhaustive swimming in the laboratory rat. *Journal of applied physiology* **21**, 1431-1434, doi:10.1152/jappl.1966.21.4.1431 (1966).

40 Vesselinovitch, S. D., Hacker, H. J. & Bannasch, P. Histochemical characterization of focal hepatic lesions induced by single diethylnitrosamine treatment in infant mice. *Cancer research* **45**, 2774-2780 (1985).

41 Zhang, X. *et al.* MicroRNA-26a is a key regulon that inhibits progression and metastasis of c-Myc/EZH2 double high advanced hepatocellular carcinoma. *Cancer letters* **426**, 98-108, doi:10.1016/j.canlet.2018.04.005 (2018).

42 Ding, M. *et al.* Melatonin prevents Drp1-mediated mitochondrial fission in diabetic hearts through SIRT1-PGC1alpha pathway. *Journal of pineal research* **65**, e12491, doi:10.1111/jpi.12491 (2018).

43 Heinz, S. *et al.* Simple combinations of lineage-determining transcription factors prime cis-regulatory elements required for macrophage and B cell identities. *Molecular cell* **38**, 576-589, doi:10.1016/j.molcel.2010.05.004 (2010).

Figures

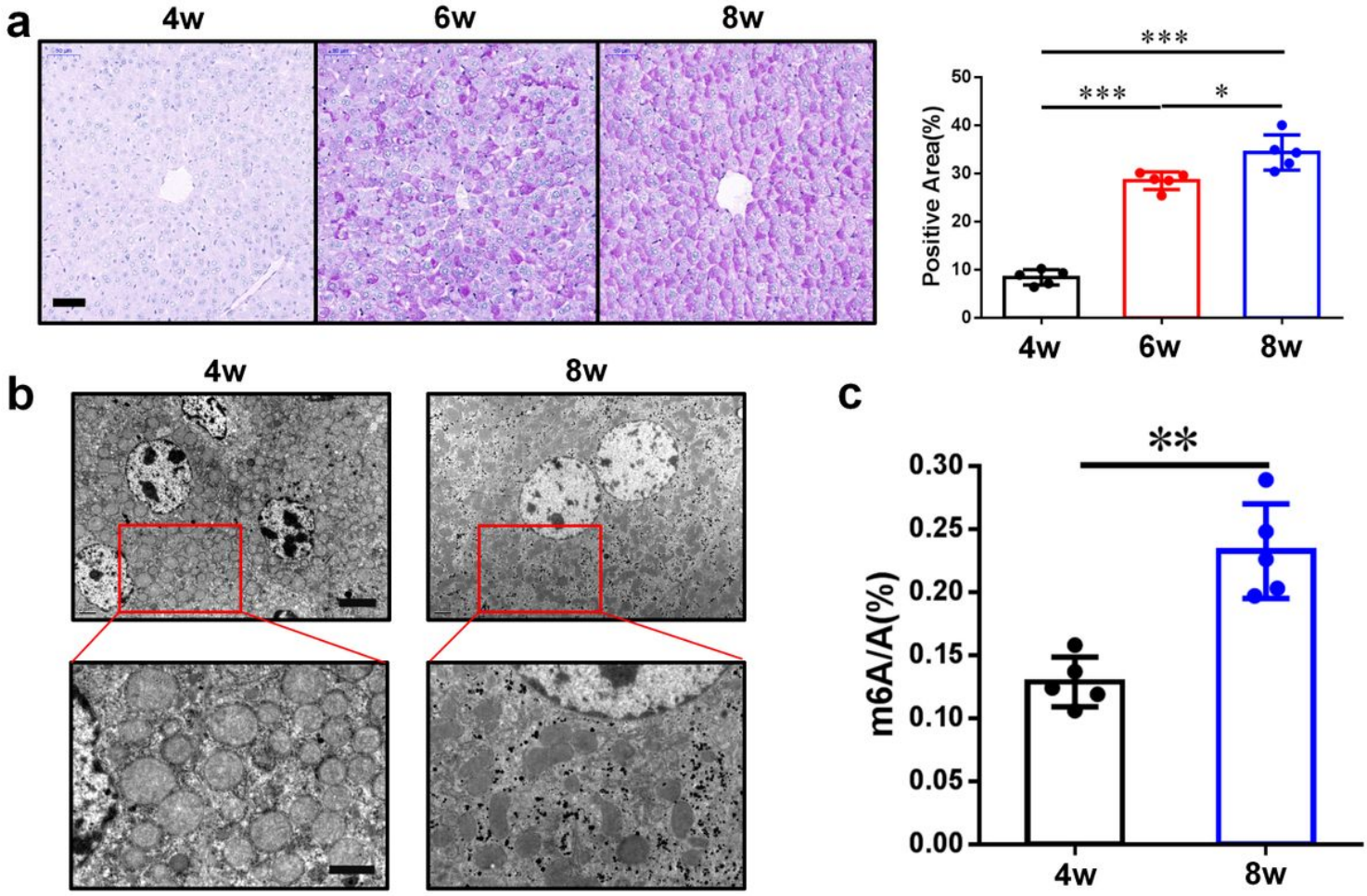

Figure 1

N6-methyladenosine modification is related to a shortage of hepatic glycogen in mouse pups. (A) PAS staining of wild-type mouse livers in different ages. The percentage of positive area is measured by Image J and shown on the right. Bar, 50μm. n≥5. (B) Transmission electron microscope pictures of wild-type mouse livers in different ages. Bar: top, 4μm; bottom, 2μm. (C) The percentage of m6A modified adenosine in total mRNA. Data are representative of at least three independent experiments and shown as mean ± SEM. (*, $p < 0.05$; **, $p < 0.01$; ***, $p < 0.001$.)

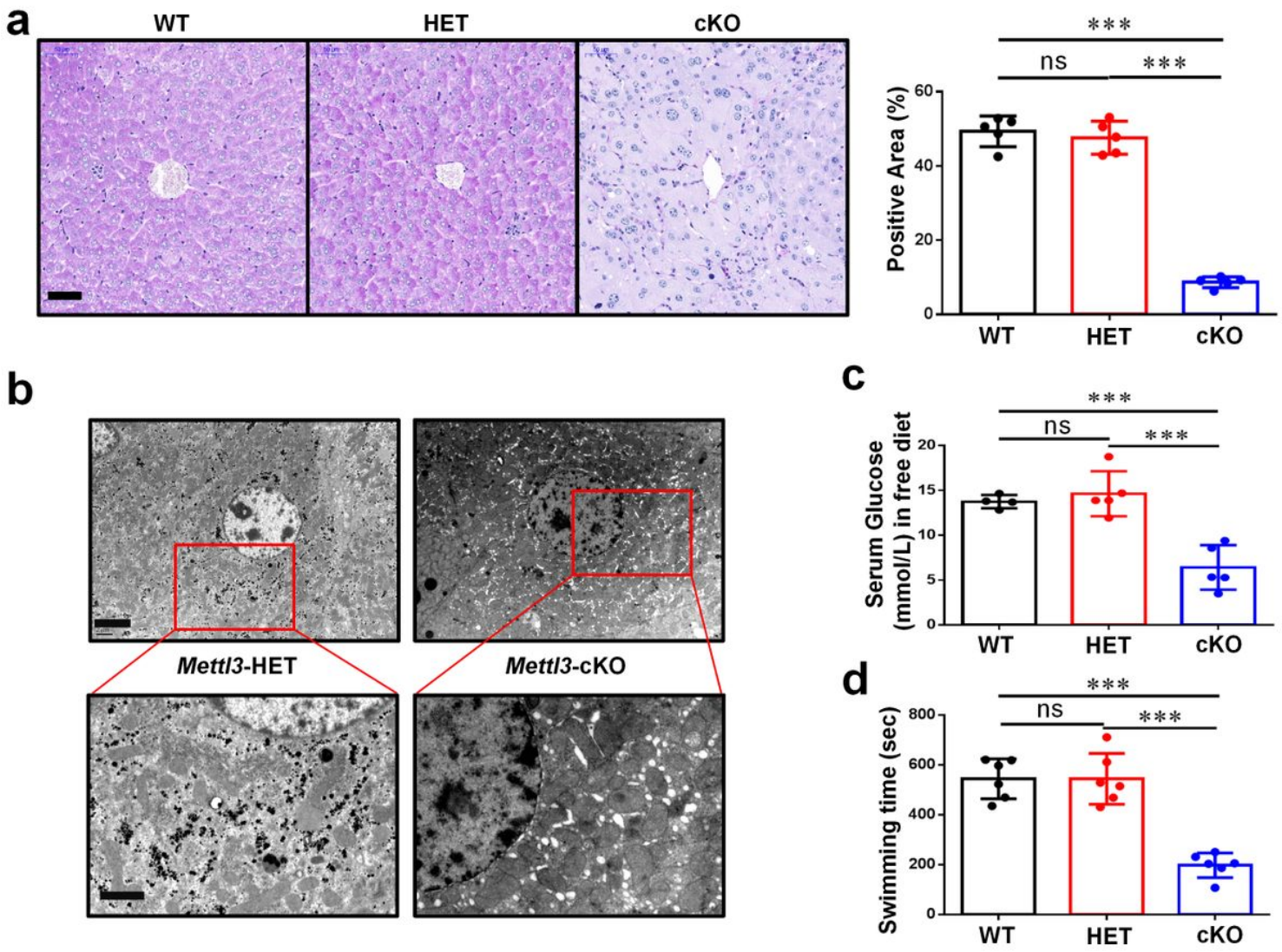

Figure 2

Mettl3 depletion simulates lack of glycogen in liver. (A) PAS staining of livers in 8-week-old mice with different Mettl3 genotypes. The percentage of positive area is measured by Image J and shown on the right. WT, wild type; HET, heterogeneous; cKO, conditional knockout (Albumin-cre). Bar, 50μm. n≥5. (B) Transmission electron microscope pictures of livers in 8-week-old mouse with different Mettl3 genotypes. Bar: top, 4μm; bottom, 2μm. (C) Serum glucose level of 8-week-old mice with different Mettl3 genotypes. (D) Exhaustive swimming assay of 8-week-old mice with different Mettl3 genotypes. Data are representative of at least three independent experiments and shown as mean ± SEM. (ns, not significant; ***, $p < 0.001$.) See also Supplementary Figure 1.

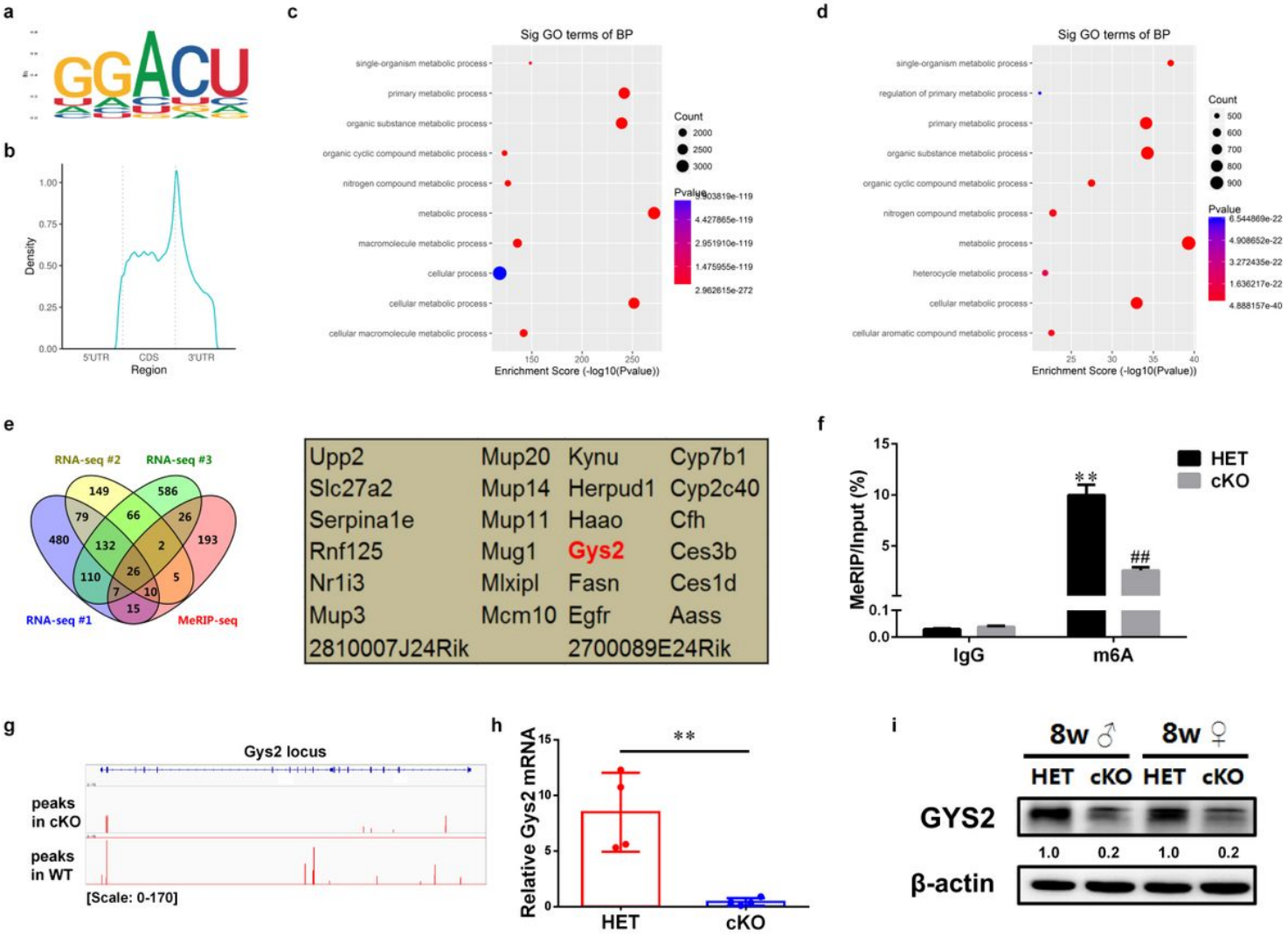

Figure 3

Identification of Gys2 mRNA by global N6-methyladenosine modification analysis as a key substrate of METTL3 in mouse liver glycogenesis. (A) The most enriched sequence motif of m6A peaks in mRNAs from 8-week-old mouse liver. p = 1e-153. (B) Distribution of m6A peaks along the 5'UTR, CDS, and 3'UTR regions of total liver mRNAs from 8-week-old control mice after normalized with length. (C, D) Significantly enriched (p-value ≤ 0.01, Benjamini–Hochberg multiple testing correction) GO terms of genes with m6A peak loss (C) and down-regulated expression (D) in Mettl3-cKO liver. (E) RNA-Seq and MeRIP-Seq identified down-regulated and m6A-lost genes in Mettl3-cKO liver comparing to control liver samples. Twenty six genes in the core intersection set are shown on the right. (F) m6A enrichment of Gys2 mRNA in mettl3-HET or cKO hepatocytes by m6A-RIP-qPCR. **, p<0.01 comparing with IgG; ##, p<0.01 comparing with HET. (G) m6A MeRIP-Seq revealed the location of specific m6A peak in Gys2 locus. (H-I) qRT-PCR (H) and western blotting (I) assay of Gys2 expression level in 8-week-old mouse livers with different Mettl3 genotypes, **, p < 0.01. Data are representative of at least three independent experiments and shown as mean ± SEM.

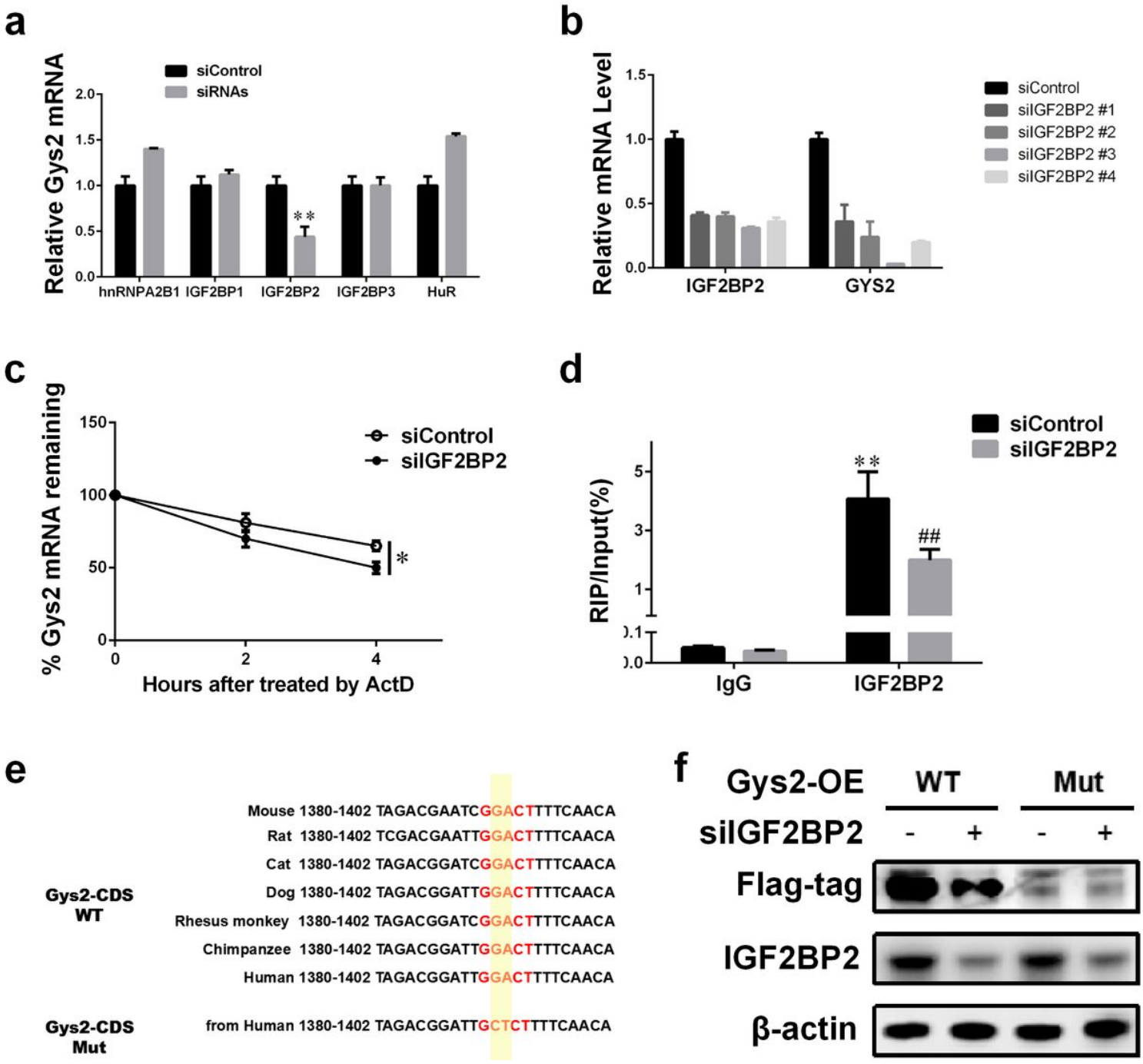

Figure 4

N6-methyladenosine stabilizes Gys2 mRNA in an IGF2BP2 dependent manner. (A) qRT-PCR assay of relative Gys2 mRNA level in siControl and indicated siRNAs. For each gene, siRNAs are mixtures of siRNA #1 and siRNA #2. **, p<0.01. (B) qRT-PCR assay of relative Igf2bp2 or Gys2 mRNA level in siControl and four different Igf2bp2 siRNAs. (C) qRT-PCR assay of Gys2 mRNA stability in siControl and siIgf2bp2 HEK-293T cells treated with actinomycin D (Act D) at the indicated times. *, p<0.05. (D) enrichment of Gys2 mRNA in siControl and siIgf2bp2 HEK-293T cells by RIP-qPCR. **, p<0.01 comparing with IgG; ##, p<0.01 comparing with HET. (E) Schematic representation of mutation in conserved coding sequence (CDS) among multiple mammals to investigate the m6A roles on Gys2 expression. (F) Flag-Gys2-CDS WT or

Flag-Gys2-CDS Mut and indicated siRNAs were transfected into HEK-293T cells for 48 h. Protein expression was measured by western blotting. Data are representative of at least three independent experiments and shown as mean ± SEM. See also Supplementary Figure 2

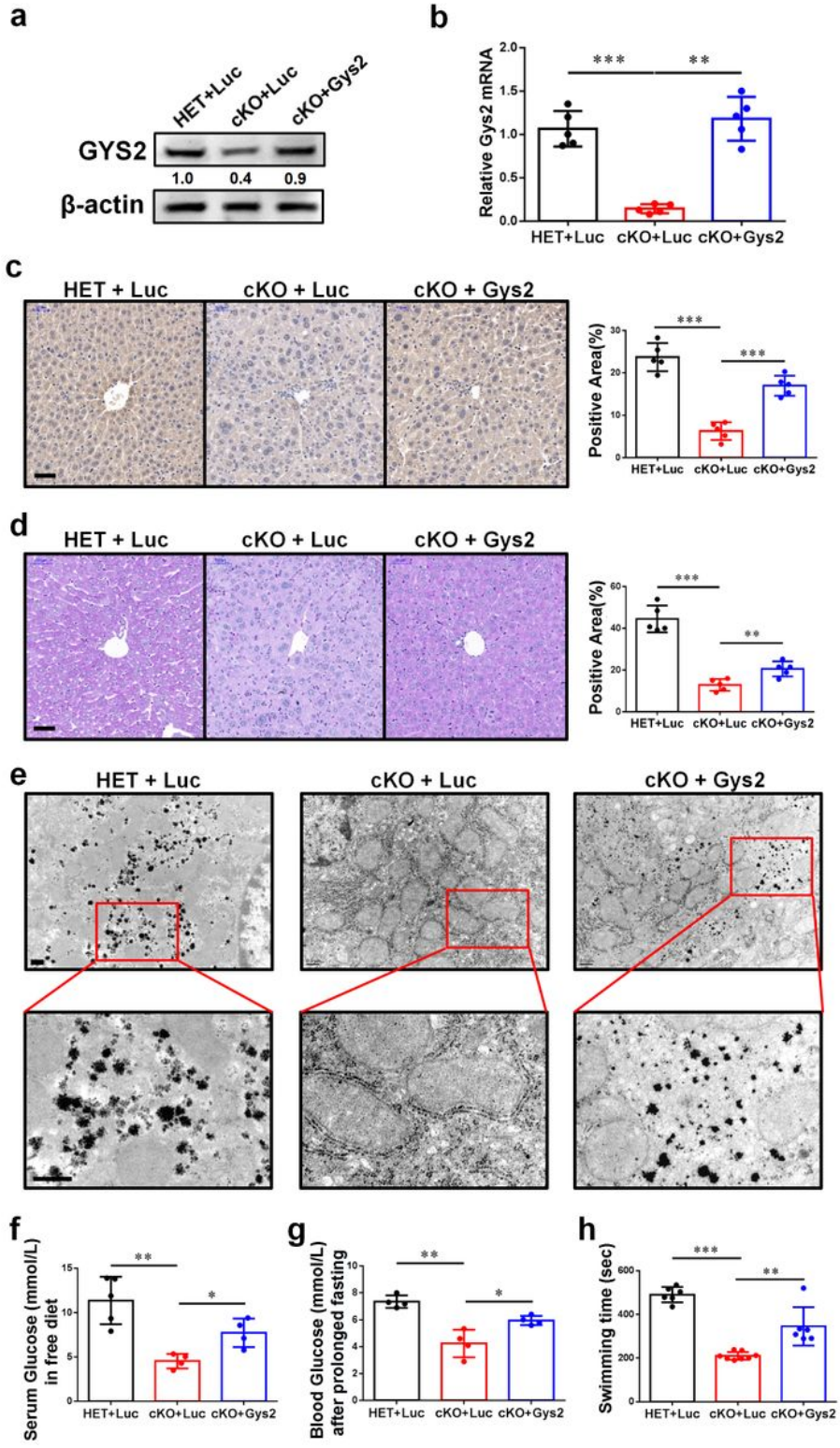

Figure 5

Reconstitution of GYS2 rescues liver glycogenesis in Mettl3-cKO mice. (A-C) Western blotting assay (A), qRT-PCR (B) and IHC staining (C) reveal the effect of reconstituted activation of GYS2. Bar, 50μm. n≥5.

(D-E) PAS staining (D) and transmission electron microscope pictures (E) of mouse livers with indicated genotypes and a luciferase (Luc) or Gys2-overexpressing adeno-associated virus (AAV). Bar: 50μm (C), 0.5μm (D). n≥5. (E) Serum glucose level of indicated groups of mice in free diet. n≥4. (F) Blood glucose level of indicated groups of mice after prolonged fasting. n≥4. (G) Exhaustive swimming assay of indicated groups of mice. n≥6. Data are representative of at least three independent experiments and shown as mean ± SEM. (*, p < 0.05; **, p < 0.01; ***, p < 0.001.)

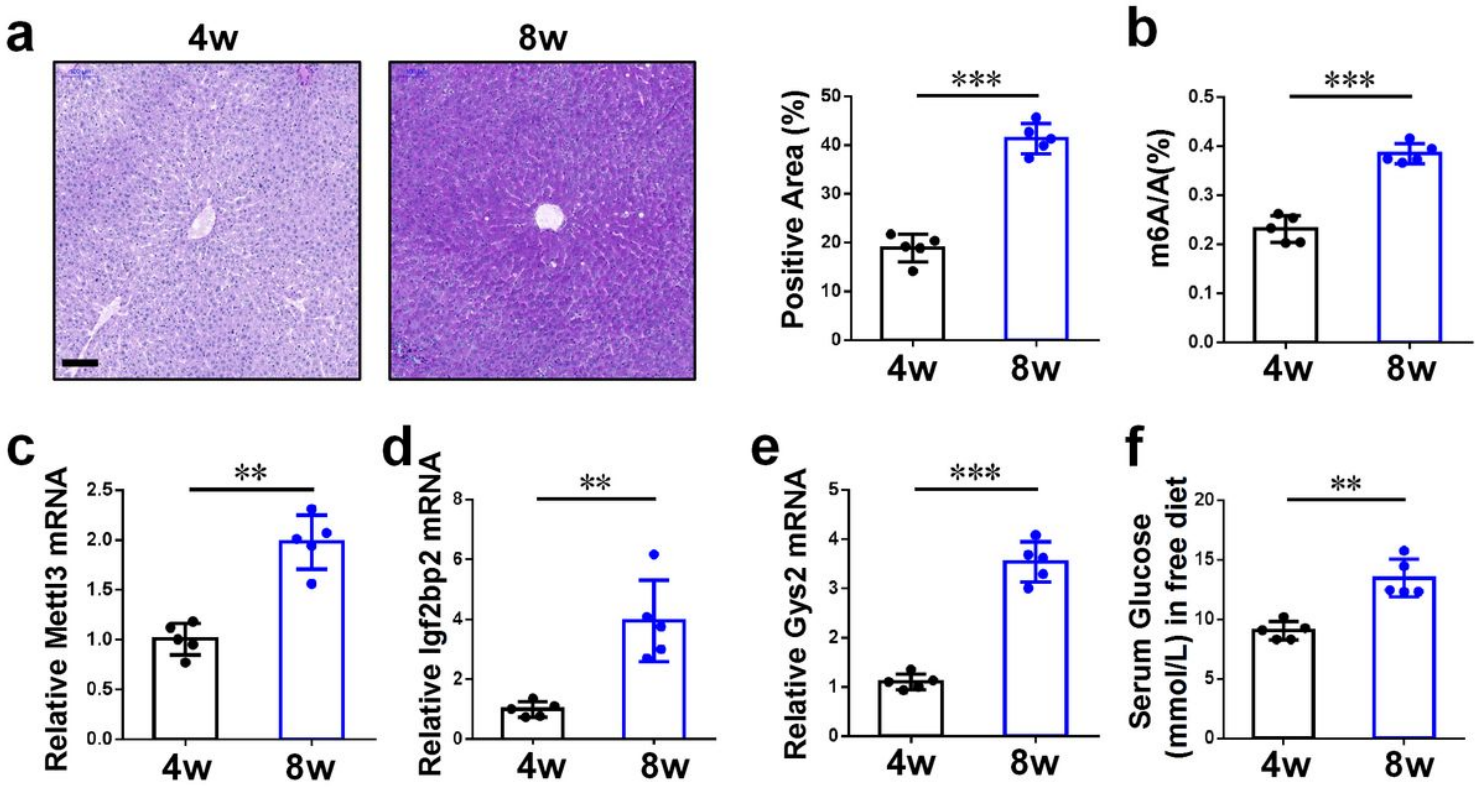

Figure 6

The METTL3-IGF2BP2-GYS2 axis is related to liver glycogen storage in rats. (A) PAS staining of wild-type rat livers in different ages. The percentage of positive area is measured by Image J and shown in the right. Bar, 100 μm. n=5. (B) The percentage of m6A modified adenosine in total mRNA of rats' livers. (C-E) qRT-PCR assay of Mettl3 (C), Igf2bp2 (D) and Gys2 (E) in rats' livers of different ages. (F) Serum glucose level of indicated age of rats in normal diet. Data are representative of at least three independent experiments and shown as mean ± SEM. (**, p < 0.01; ***, p < 0.001.)

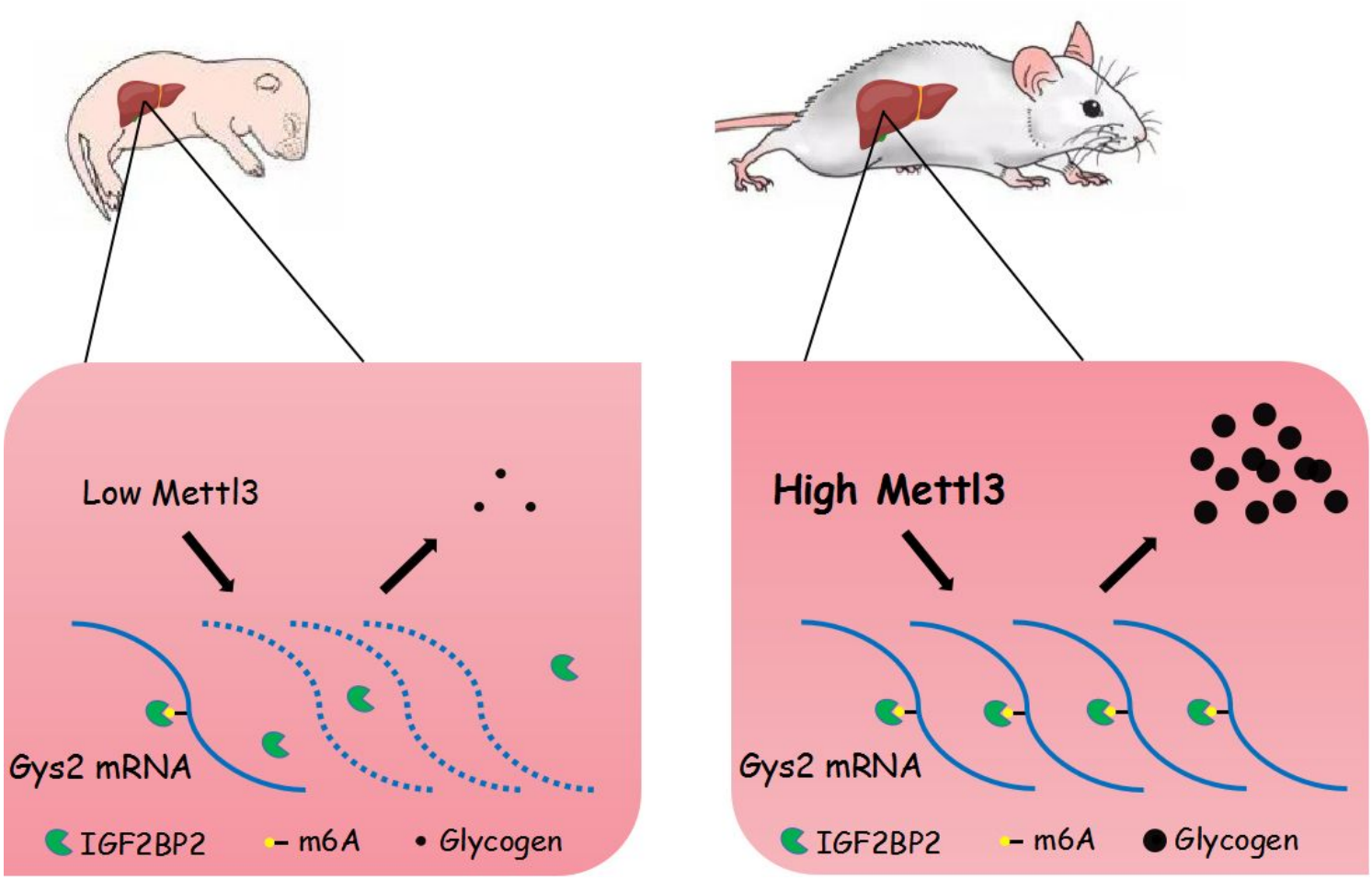

Figure 7

Working model of our study.

Supplementary Files

This is a list of supplementary files associated with this preprint. Click to download.

- SupplementaryData.docx